On the dynamic determinants of reproductive failure under drought in maize

Carlos D Messina, Graeme L Hammer, Greg Mclean, Mark Cooper, Erik J van Oosterom, François Tardieu, Scott C Chapman, Alastair Doherty, Carla Gho

in silico Plants

OXFORD UNIVERSITY PRESS

Original Research

On the dynamic determinants of reproductive failure under drought in maize

Carlos D. Messina[1*], Graeme L. Hammer[2], Greg McLean[3], Mark Cooper[2], Erik J. van Oosterom[2], Francois Tardieu[4], Scott C. Chapman[5], Alastair Doherty[2] and Carla Gho[6]

[1]Agriculture Division of DowDuPont, Corteva Agriscience, 7250 NW 62nd Avenue, Johnston, IA 50131, USA
[2]Queensland Alliance for Agriculture and Food Innovation, Centre for Crop Science, The University of Queensland, Brisbane, Queensland 4072, Australia
[3]Department of Agriculture and Fisheries, Agri-Science Queensland, 203 Tor Street, Toowoomba, Queensland 4350, Australia
[4]Laboratoire d'Ecophysiologie des Plantes sous Stress Environnementaux – Bât. 7, INRA, UMR 759, 2 Place Viala, 34060 Montpellier, France
[5]CSIRO Agriculture & Food, Queensland Bioscience Precinct, 306 Carmody Road, St Lucia, Queensland 4067, Australia
[6]Agriculture Division of DowDuPont, Corteva Agriscience, 1609 Buin, Chile

Received: 2 February 2019 **Editorial decision:** 5 April 2019 **Accepted:** 15 May 2019

Citation: Messina CD, Hammer GL, McLean G, Cooper M, van Oosterom EJ, Tardieu F, Chapman SC, Doherty A, Gho C. 2019. On the dynamic determinants of reproductive failure under drought in maize. *In Silico Plants* **2019**: diz003; doi: 10.1093/insilicoplants/diz003

Abstract. Reproductive failure under drought in maize (*Zea mays*) is a major cause of instability in global food systems. While there has been extensive research on maize reproductive physiology, it has not been formalized in mathematical form to enable the study and prediction of emergent phenotypes, physiological epistasis and pleiotropy. We developed a quantitative synthesis organized as a dynamical model for cohorting of reproductive structures along the ear while accounting for carbon and water supply and demand balances. The model can simulate the dynamics of silk initiation, elongation, fertilization and kernel growth, and can generate well-known emergent phenotypes such as the relationship between plant growth, anthesis-silking interval, kernel number and yield, as well as ear phenotypes under drought (e.g. tip kernel abortion). Simulation of field experiments with controlled drought conditions showed that predictions tracked well the observed response of yield and yield components to timing of water deficit. This framework represents a significant improvement from previous approaches to simulate reproductive physiology in maize. We envisage opportunities for this predictive capacity to advance our understanding of maize reproductive biology by informing experimentation, supporting breeding and increasing productivity in maize.

Keywords: Anthesis-silking interval (ASI); assimilate partitioning; crop growth model (CGM); ear phenotypes; fertilization; grain cohorts; kernel abortion; water deficit.

Introduction

Reproductive failure in maize (*Zea mays*) has far-reaching societal consequences (Cane *et al.* 1994; Ray *et al.* 2013, 2015). Instability in maize price associated with the 2012 drought in the USA and subsequent favourable years disrupted global grain trade (Boyer *et al.* 2013). Understanding the reproductive physiology of maize can inform policies to increase genetic gain for yield, water productivity and stability of food systems (Hammer *et al.* 2006; Messina *et al.* 2011; Ray *et al.* 2013; Cooper *et al.*

*Corresponding author's e-mail address: charlie.messina@corteva.com

2014). However, this understanding needs to be quantitative and able to capture the interplay between genetics and agronomic management for it to be applied in systems for crop design, forecasting and breeding (Cooper *et al.* 2014; Hammer *et al.* 2014; Messina *et al.* 2018).

Yield losses in maize are most pronounced when stress occurs during flowering (Claassen and Shaw 1970; Campos *et al.* 2006). But events that are not visibly obvious prior to silk emergence and fertilization may prevent pollination or predispose the kernels to post-fertilization reproductive failure (Moss and Downy 1971; Cárcova and Otegui 2001; Cárcova *et al.* 2003; Oury *et al.* 2016). Reproductive development, carbohydrate availability and hydraulic limitations have been implicated in pollination failure due to restricted silk elongation, developmental asynchrony and early kernel abortion unrelated to fertilization (Herrero and Johnson 1981; Hall *et al.* 1982; Westgate and Boyer, 1985a,b, 1986; Edmeades *et al.* 1993; Cárcova and Otegui, 2001, 2007; Fuad Hassan *et al.* 2008; Turc *et al.* 2016). The fraction of ovaries that develop into grains is influenced by differential development of ovary cohorts along the ear (Otegui and Melon 1997), the pattern of silk emergence and the simultaneous arrest of silk growth across all ovaries (Oury *et al.* 2016). Reduced photosynthesis, carbohydrate reserves, glucose gradient and carbohydrate flux at low water potentials have been implicated in embryo abortion (Zinselmeier *et al.* 1995, 1999). The effects of timing of water deficit and pattern of zygote development along the ear row (cohorts) determine the nature of the ear phenotype associated with reproductive failure (Fig. 1).

There is a legacy of research on the physiological determinants of kernel set in maize (Boyer 1996; Saini and

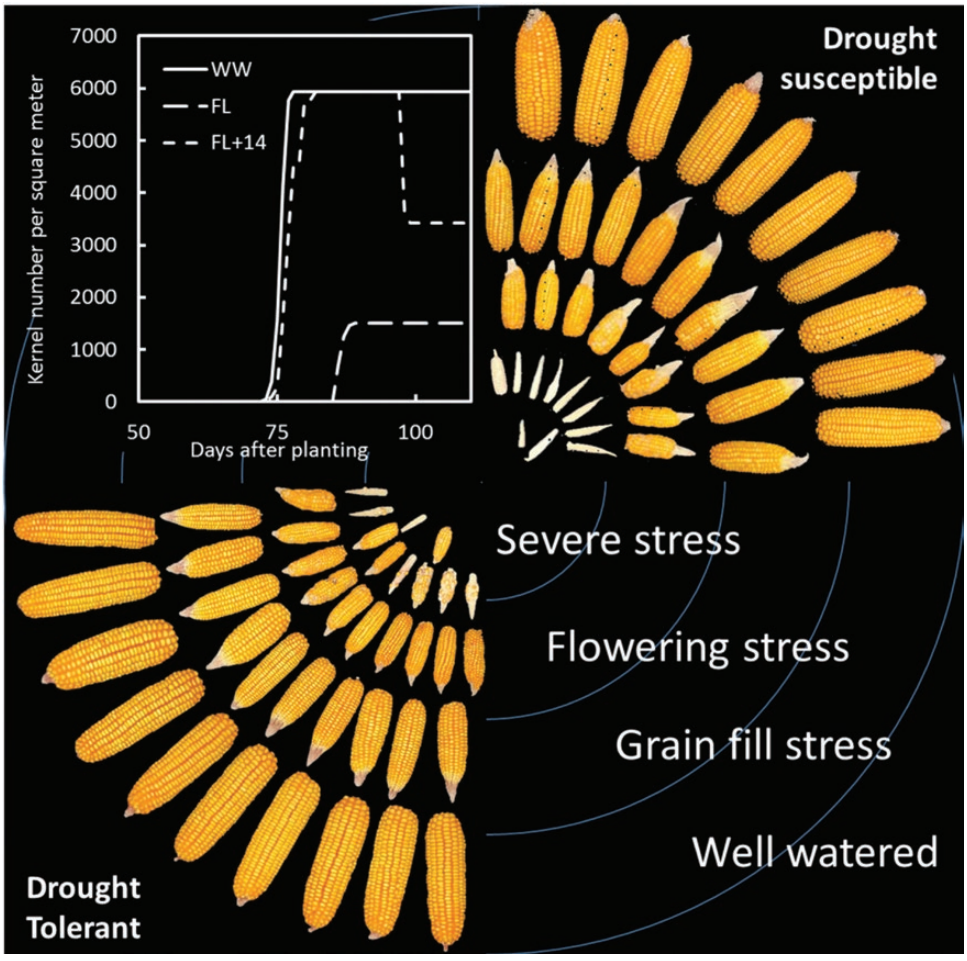

Figure 1. Ear phenotypes observed with different timing of water deficit generating reproductive failure for two hybrids that contrast in response to drought. A simulation of kernel number per m^2 under three water deficit scenarios is shown for reference to timing of stress and impact on kernel set. The outer band shows the ear phenotype for a plant grown without water deficit (Well watered). The next three bands show the phenotype associated with (i) water deficit after silking and early grain fill (Grain fill stress; tip kernel abortion due to carbohydrate starvation of fertilized florets), (ii) water deficit during flowering (Flowering stress; short ear due to reduced silk elongation and emergence) and (iii) severe water deficit starting pre-flowering (Severe stress; barrenness (scatter grain) due to lack of silk emergence and fertilization).

Westgate 2000). However, it has not been formalized in mathematical form to enable the study and prediction of reproductive failure caused by dynamic aspects of the biological system. Here we develop a quantitative synthesis of the current understanding of the reproductive physiology of maize in the form of a simulation model that captures the dynamics of the determinants underpinning kernel set. A key feature of the model is the framework for cohorting of reproductive structures based on the temporal variation of silk initiation and extension, fertilization and initiation of kernel growth (Fig. 2). The cohorting enables simulation of the phenotypes associated with reproductive failure by considering differential effects of timing of water deficit on processes for each cohort, e.g. supply of carbohydrates. The integration of the model within a crop modelling platform (Holzworth *et al.* 2014) enables the study and prediction of reproductive failure as an emergent property of system dynamics at the crop scale (Messina *et al.* 2009; Soufizadeh *et al.* 2018), which is a distinctive characteristic from earlier models such as those proposed by Lizaso *et al.* (2007) and Borrás *et al.* (2009).

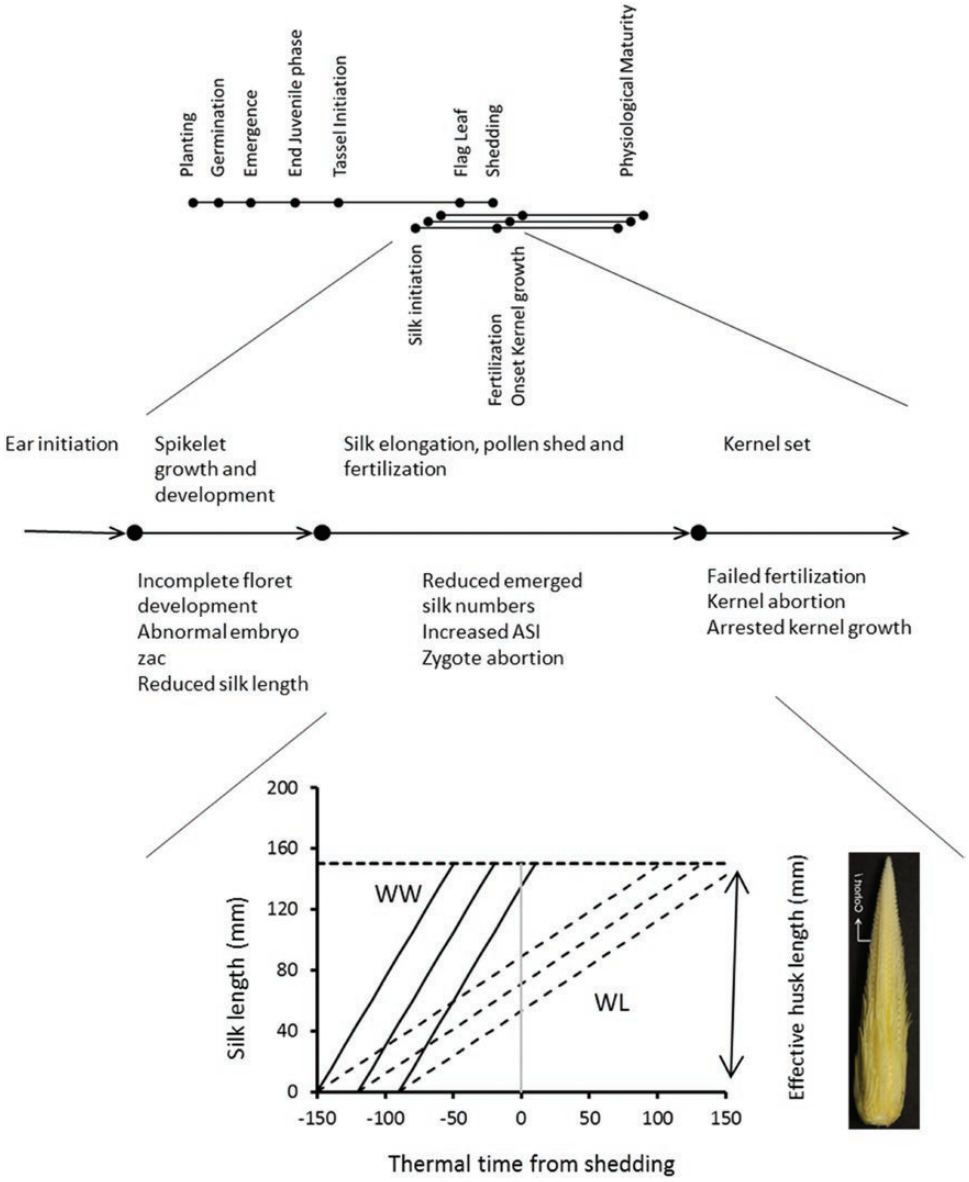

Figure 2. Framework for maize reproductive biology model within crop life cycle. Solid lines indicate passage through developmental phases for the main culm (planting to anthesis/pollen shedding) and for the cohorts of florets generated on the ear (silk initiation to grain maturity). The potential impacts of water deficit at specific stages on reproductive failure are indicated. The lower schematic depicts the elongation of cohorts of silks under well-watered (WW—solid lines) and water-limited (WL—broken lines) conditions. Silk emergence is estimated as the time that the silk length of each cohort reaches the effective husk length.

We evaluate the model by means of simulation and experimentation under controlled patterns of water deficit. The integrated model can generate emergent phenotypes characteristic of reproductive failure under drought, and reproduce well-known empirical relationships used to predict kernel set and yield in maize, for example—

- anthesis-silking interval (ASI) and yield,
- silk number and ear mass at silking,
- kernel number and plant growth rate around anthesis.

We provide a perspective on future opportunities for the application of the unified framework to advance plant science, enhance predictive breeding and agronomy and increase productivity in maize.

Model Description

Crop growth and soil and water environment simulation framework

Crop growth models are mathematical representations of the plant-soil-atmosphere system coded in software to enable analyses of plant and cropping systems (Messina *et al.* 2009; Wallach *et al.* 2018). The integration of the plant or crop module within a framework that contains algorithms to simulate water and N balances in the soil and atmospheric processes, enables the application of these systems to crop design in the context of a cropping system (Hammer *et al.* 2014), the translation of biological knowledge at the genetic level to the crop system level at regional and national scales (e.g. Hammer *et al.* 2006; Messina *et al.* 2018), simulation of breeding strategies (Messina *et al.* 2009), evolution in fitness landscapes (Messina *et al.* 2011) and more recently genomic prediction (Cooper *et al.* 2014; Messina *et al.* 2018).

Here we use the APSIM (Agricultural Production systems SIMulator) modelling platform (Holzworth *et al.* 2014) as a scaffold to produce a quantitative synthesis of maize reproductive biology. APSIM contains crop, soil, management and weather modules structured around an interface engine that is designed to manage the connections among process modules, while performing the mathematical computations for the specified system simulation. The process modules encapsulate the biological knowledge for different crops and soil and atmospheric processes. Recent development of the plant module for sorghum (Hammer *et al.* 2010) facilitates the use of this model for genetic studies. The maize module in APSIM has been updated recently in a similar manner (Soufizadeh *et al.* 2018). These crop modules are constructed from a library of interacting submodules accounting for crop growth and development processes (Holzworth *et al.* 2014). The reproduction biology submodule developed here substituted for the existing kernel set submodule. Software and model code is available through the APSIM Initiative (http://www.apsim.info/) for non-commercial purposes.

Overview of the reproductive growth and development simulation framework

The model proposed provides a dynamic framework for the cohorting of reproductive structures (silks, zygotes, kernels) based on the dynamics of silk initiation, silk extension, pollination and kernel growth (Fig. 2). The maximum number of florets is set as a genotypic factor dependent on potential kernel size and potential total kernel weight per plant (Soufizadeh *et al.* 2018). The assumption of a relationship between ovule size, pericarp expansion and kernel size is based on Saini and Westgate (2000). The dynamic approach accounts for effects of both hydraulics and carbohydrate availability on kernel set. Silks cannot be pollinated until they emerge from the husk. The model is structured around the elongation of silks and the time it takes for silks to emerge from the husk tip. For different cohorts of flowers, silk length at emergence from the husk tip is determined by the growth of the ears and husks, and the position of silks within the ear. In general, upper silks (later cohorts) are shorter when they appear relative to lower silks (earlier cohorts) (Cárcova *et al.* 2003). The temporal distribution of silk appearance also depends on the severity of water deficit (Fuad Hassan *et al.* 2008; Turc *et al.* 2016). In the absence of water deficit, silks elongate rapidly and emerge within a narrow window of time (Fig. 2), whereas with water deficit silk appearance is delayed (generating longer ASI) and silks emerge over a longer period (Fig. 2). As a first approximation, a fixed threshold of the silk length needed for silk appearance is assumed in the model for all cohorts, although this length threshold can be varied among genotypes. In addition, the silk initiation rate (i.e. number of silks initiated per unit of thermal time), the potential silk elongation rate and the response of silk elongation to water deficit are given as genotypic constants. Each cohort of silks is allowed to initiate, age and extend until it emerges and is available to be pollinated.

The availability of pollen at any time follows a Gaussian distribution centred shortly after the time of anthesis/shedding of the main culm (Fig. 2) (Uribelarrea *et al.* 2002). Viability of pollen can be affected by high temperature at the time of pollination (Schoper *et al.* 1987). Water deficit acts to trigger floret or kernel abortion through delayed silk elongation that is either

sufficient to restrict silk emergence completely or induce asynchronous pollination across cohorts. The cohorts of kernels arising from silks that are pollinated on any particular day grow at a potential rate determined by an expolinear growth function. Reduction in carbohydrate availability, which might also be associated with water deficit, can restrict kernel growth rate and ultimately trigger abortion. Because of the cohort structure, it is possible to implement a scheme of competition for available carbohydrates whereby the first cohort has priority in allocation. This can lead to the abortion of kernels set from late emerged silks nearer the tip of the ear. Access to stored carbohydrates to support kernel and ear growth at all stages is implemented assuming a remobilization rate from stem and husks that follows first-order kinetics and depends on sink strength. The sink strength in turn is dependent on kernel and ear size, which determine their potential growth rate.

Detail of the reproductive growth and development simulation framework

The degree day (°Cd) concept (D) is used here to model physiological age and development in flowering and silking. It represents the thermal units accumulated above a base temperature (T_b, **see Supporting Information—Table S1**). Cardinal temperatures for development are 8, 34 and 40 °C for the minimum, optimum and maximum temperatures, respectively (Birch *et al.* 1998a,b), with an adjustment for temperatures between 0 and 18 °C, for which thermal units increase linearly from 0 to 10 (Wilson *et al.* 1995).

The onset of silk initiation and the linear silk elongation phase in the ear is a characteristic of a genotype and it is defined here, for reference, as 150 °Cd before anthesis and pollen shedding from the tassel at the terminal apex (Cárcova *et al.* 2003). All silks are initiated over a 60 °Cd interval generating a cohort-age structure over time. The silk initiation rate is the total number of silks divided by this initiation interval. Silk elongation rate, the daily (t) change in silk length (L) (Eq. 1), is modelled as a function of temperature (T) and daily crop water status, indexed by the crop water supply (S) to demand (D_e) ratio (SD) (Herrero and Johnson 1980; Westgate and Boyer 1985a; Bassetti and Westgate 1993; Fuad Hassan *et al.* 2008; Turc *et al.* 2016). Sensitivity to temperature is determined by one empirical constant (ϑ) that implements a constitutive development rate (1.5 mm °Cd^{-1}) and T_b, temperature below which development ceases. The parameter γ is included to account for genetic variation in the sensitivity of silk elongation to water deficit (Turc *et al.* 2016).

$$L(t) = \vartheta(T - T_b)(1 - \gamma(1 - SD)) + L(t-1) \qquad (1)$$

The effective silk length (ESL, Fig. 2) is defined as the silk length at silk emergence from the husk. Here, it is taken as the average across all silks for an ear, so it is the distance between the midpoint of a silking ear lengthwise and the tip of the husk cover. A standard ESL of 15 cm, which is based on an average potential silk elongation rate of 1.5 mm °Cd^{-1}, and 100 °Cd duration from start of silk elongation until silk appearance (Cárcova *et al.* 2003), can be varied to allow for genotypic variation.

In the absence of pollination, silks start to senesce but retain the capacity to support pollen germination and pollen tube growth. Fertilization is prevented when the base of the silk collapses. Florets remain fertile for a period of 7–10 days or 150 °Cd after appearance (Bassetti and Westgate 1993). Because silk appearance takes a minimum of 100 °Cd after initiation of silk elongation, this means that floret fertility starts to decline after 250 °Cd from initiation. A consequence of a delay in silk appearance under drought is the shortening of the period of silk fertility. Silk fertility declines to 0 by around 350 °Cd after silk initiation. In Eq. 2, the degree day concept is used to model silk ageing and fertility ($r(t)$) using a sigmoid function, which can also be implemented as a bilinear approximation. The parameters φ and D_0 are empirical constants included to model genetic variation in the temporal change of fertility with age as shown by Anderson *et al.* (2004).

$$r(t) = \frac{1}{1 + e^{\varphi(D - D_0)}} \qquad (2)$$

Pollen availability can affect kernel set when stress affects timing of silk emergence and/or high temperatures decrease pollen supply and viability (Herrero and Johnson 1980; Schoper *et al.* 1987; Bassetti and Westgate 1994). Fertilization is simulated when pollen is available and fertile. Pollen availability at t days after shedding, $p(t)$, is modelled assuming a Gaussian distribution centred on τ days after shedding (Uribelarrea *et al.* 2002) (Eq. 3),

$$p(t) = \alpha e^{-0.5 \times \left(\frac{t - \tau}{\sqrt{\beta}}\right)^2} \qquad (3)$$

The parameters α, β and τ describe the distribution of pollen number (p) with respect to days after shedding (Uribelarrea *et al.* 2002).

High temperature can reduce total pollen viability (Herrero and Johnson 1980; Schoper *et al.* 1987). This effect on pollen viability at any time, $v(t)$, is modelled using a sigmoid function, which can also be implemented as a bilinear approximation (Eq. 4).

$$v(t) = \frac{1}{1 + e^{\rho(D_H - D_{0H})}} \qquad (4)$$

The input to this function is the accumulated sum of daily maximum temperature greater than a threshold,

here set at 35 °C and denoted as D_H, during a developmental window of 150 °Cd prior to shedding. The parameters ρ and D_{0H} are empirical constants included to model genetic variation in pollen susceptibility to heat stress (Herrero and Johnson 1980) in a similar manner to that for sorghum (Singh *et al.* 2017).

The final number of pollen grains available for pollination results from the product of Eqs. 3 and 4. Previous studies indicate an absence of detrimental effects of drought on pollen germination (Herrero and Johnson 1981). The limitation of viable pollen for fertilization is modelled considering that kernel set is not restricted when pollen number is >200 grains per cm^2 (Bassetti and Westgate 1994; Uribelarrea *et al.* 2002). When fertile pollen availability is less than this threshold a pollination multiplier that declines linearly from 1 to 0 with pollen number is implemented to reduce fertilization.

On each day, kernel number increases depending on the number of silks that have appeared but not been previously pollinated, their silk fertility (Eq. 2) and the pollen factors (Eqs. 3 and 4). If fertile pollen availability is not sufficient to fertilize all exposed silks, then pollination of older silks occurs first. Because silks that emerged at time t but are not pollinated are, at least in the model, longer than silks emerging at time $t + 1$, these older silks are preferentially pollinated. Any fertile silks that remain unpollinated at time t are added to the pool of silks that can emerge at $t + 1$. Consequently, this implementation can result in kernels within a ring on the ear that have a different age (date of pollination). Scatter grain can also occur as an emergent phenotype, but only when silk emergence is delayed (long ASI) under severe stress.

An important concept underlying the model is that cob growth, which occurs during the period of kernel set and early kernel growth, is dependent on both constitutive and dynamic factors. Constitutive expression of potential number of florets (Edmeades *et al.* 1993; Cárcova *et al.* 2003), potential kernel weight (PKW; Gambín *et al.* 2008) and kernel to cob ratio (ω) determines the potential size of the cob. Dynamic factors that regulate cob growth rate are silk appearance, which determines the realized number of silks (SN) that could be fertilized, fertilization of these as affected by pollen availability and viability, and silk fertility. The maximum number of silks defined at the outset is consistent with the product of kernels per row and rows per ear. In the absence of fertilization, cob growth is assumed to be arrested. The maximum mass of the cob at any time of development ($We_m(t)$) is then determined as,

$$We_m(t) = SN_t \times \frac{1}{\omega} \times PKW \tag{5}$$

The actual cob mass at any point in time ($We(t)$) is modelled as a function of thermal time (D; D_b see below) to account for the environmental effect of temperature on plant development and the maximum cob mass, but is not influenced by carbon availability (Edmeades *et al.* 1993),

$$We(t) = \frac{We_m(t)}{1 + e^{\left(D - \frac{D_b}{2}\right)}} \tag{6}$$

Prior to anthesis and coinciding with the onset of silk initiation (i.e. 150 °Cd before shedding), cob growth is assumed to commence and proceed at 1/150 g $°Cd^{-1}$, which gives a reference ear mass of 1 g at anthesis, as found for an adapted temperate maize hybrid (Cooper *et al.* 2014). Ear mass at pollination will thus depend on timing of pollination, with a slightly greater value resulting if pollination is delayed.

Potential kernel growth is modelled for each cohort of kernels (i) via an expolinear growth function (Eq. 7). A cohort is defined by the silks that are pollinated at a given time t and can thus comprise more than one ring of kernels on the ear. The expolinear function for potential kernel growth rate within a cohort depends on (i) thermal time, starting at pollination to account for effects of temperature on kernel growth and development (Muchow 1990; Kiniry and Bonhomme 1991), (ii) a maximum growth rate (PKGR), (iii) the thermal time taken to reach 50 % PKGR (D_b) and (iv) a constant (rm) that determines the rate at which the kernel growth rate transitions from exponential to linear growth. PKGR is determined from the given PKW and the thermal time to physiological maturity (D_{pm}) less an allowance for the initial lag phase in grain growth after pollination,

$$k_{i,t} = \frac{e^{rm \times (D_i - D_b)}}{1 + e^{rm \times (D_i - D_b)}} \tag{7A}$$

$$PKGR_t = k_{i,t} \times PKGR \tag{7B}$$

$$PKGR = \frac{PKW}{D_{pm} - 170} \tag{7C}$$

The actual kernel growth rate for a cohort of kernels can be restricted by the availability of carbohydrates. Supply of these to the ear at any point in time ($S(t)$; Eq. 8) is calculated from current carbon net assimilation through photosynthesis ($Pg(t)$) and the amount of carbohydrates that could be mobilized from stem ($Ws(t)$) at rate ϕ. Because mobilization rate is dependent on sink activity, this rate was modelled as a function of the number of growing kernels per cohort (KN_i) integrated over cohorts, their sink strength as determined by their kernel growth rate ($k_{i,t}$; Eq. 7), and the cob growth rate ($\Delta We(t)$) relative to its maximum growth, $\xi We_m(t)/4$, which is derived

from the derivative of Eq. 6 assuming that cob maximum growth occurs at thermal time $D_b/2$,

$$S(t) = \mathrm{Pg}(t) + \left(\frac{\sum \mathrm{KN}_i \times k_{i,t}}{\sum \mathrm{KN}_i} + \frac{4 \times \Delta\mathrm{We}(t)}{\xi \times \Delta\mathrm{We}_m(t)} \right) \times \mathrm{Ws}(t) \times \phi \quad (8)$$

Under stress conditions, remobilization from stems and leaves at silking is virtually 0 (Westgate and Boyer 1985b). At silking stage of development, kernel growth and growth of the cob contribute little to the sink strength term. Sink strength increases with the progression of development and enhances the potential contribution of carbon reserves to maintaining kernel growth during grain filling. When supply is greater than the demand for carbohydrates, kernel growth is unrestricted and proceeds at the potential rate (Eq. 7). Otherwise, the actual kernel growth rate for any cohort (AKGR_i) is calculated using a recurrent algorithm (Eq. 9) that determines assimilate available to that cohort,

$$\mathrm{AKGR}_i = S(t) - \Delta\mathrm{We}(t) - \sum_{i=1}^{i-1} \mathrm{KN}_i \times \mathrm{PKGR}_i \quad (9)$$

The actual kernel weight within each cohort is determined by the numerical integration (Eq. 10) of the kernel growth rate (KGR_i) for that cohort,

$$\mathrm{KW}_{i,t} = \mathrm{KW}_{i,t-1} + \mathrm{KGR}_{i,t} \quad (10)$$

with an upper bound given by the PKW set for the genotype (Gambín *et al.* 2008). Within a cohort, all kernels are assumed equal. Consequently, if for cohort *i* the assimilate supply is smaller than the kernel demand for growth (Eq. 9), then KGR_i is reduced equally for all kernels. This approximation is supported by experimentation showing reduced abortion when pollination is synchronized (Cárcova *et al.* 2000).

Kernel abortion occurs when AKGR does meet criteria that define zygote starvation and death. Kernel abortion within a cohort is simulated whenever both of the following criteria are met for *N* consecutive days, currently set at 3,

$$\begin{cases} \mathrm{KGR}_i = 0 \\ \mathrm{KW}_{i,t} < 0.15 \times \mathrm{PKW} \end{cases} \quad (11)$$

in which case the whole cohort is considered to abort and kernel per ear (KPE) is revised as,

$$\mathrm{KPE}_t = \mathrm{KPE}_{t-1} - \mathrm{KN}_{i,t} \quad (12)$$

Model evaluation and testing

A number of functional relationships have been proposed to predict kernel set in maize. These phenomenological relationships were proposed to help understand the effects of changes in agronomic practices and environmental variation on grain yield (Andrade *et al.* 1999; Borrás *et al.* 2007; Soufizadeh *et al.* 2018), use of secondary traits as a means to improve genetic selection (Bolaños and Edmeades 1996; Cooper *et al.* 2014) and understanding of the underpinning biological process of reproductive failure (Hall *et al.* 1982; Vega *et al.* 2001; Oury *et al.* 2016). Because delay in silk appearance in response to water deficit is a common feature across these published methods, we integrated the more process-based model defined in Eqs. 1–12 within the maize crop growth and development model in APSIM (Holzworth *et al.* 2014; Soufizadeh *et al.* 2018), and conducted simulations under various levels and timing of water deficit. The model was evaluated for its capacity to simulate known phenotypic relationships and responses as emergent consequences of the model dynamics. Specifically, we sought to test the ability of the model to generate the impact of water deficit on kernel set due to delay in silking relative to anthesis, and for its capacity to reproduce the associations between ASI and yield, ear mass and silk number, and crop growth rate and kernel number.

A structured simulation experiment with four scenarios of water deficit was designed to generate data sets for this qualitative model evaluation. The simulation experiment was conducted for a semi-arid environment in central Chile (33.90°S, 70.77°W) with full control of irrigation. Irrigation management was specified so as to generate three scenarios of water deficit with similar levels of intensity but occurring at different developmental stages: flowering (fl), 1 week after flowering (fl+7) and 2 weeks after flowering (fl+14) (Fig. 3). The simulated crop was planted on 7 November 2001 at a rate of 9.0 plants per m^2 and 76 cm between planting rows on a silt loam soil with a depth of 1.50 m and plant-available water capacity of 240 mm. Maize hybrid parameterization was the same as that detailed in Hammer *et al.* (2009), together with the values for additional coefficients required for the cohort model as given in **Supporting Information—Table S1**.

Results

Simulating silking dynamics, ASI and kernel set under water deficit

The structured simulation experiment with four scenarios of water deficit generated various levels of timing and severity of water deficit (Fig. 3) as indicated by the temporal dynamics of the water supply to demand ratio. The well-watered scenario had minimal water deficit (SD ratio near 1 throughout), while in other scenarios, the maximum water deficit (SD ratio ~0.2) occurred either at

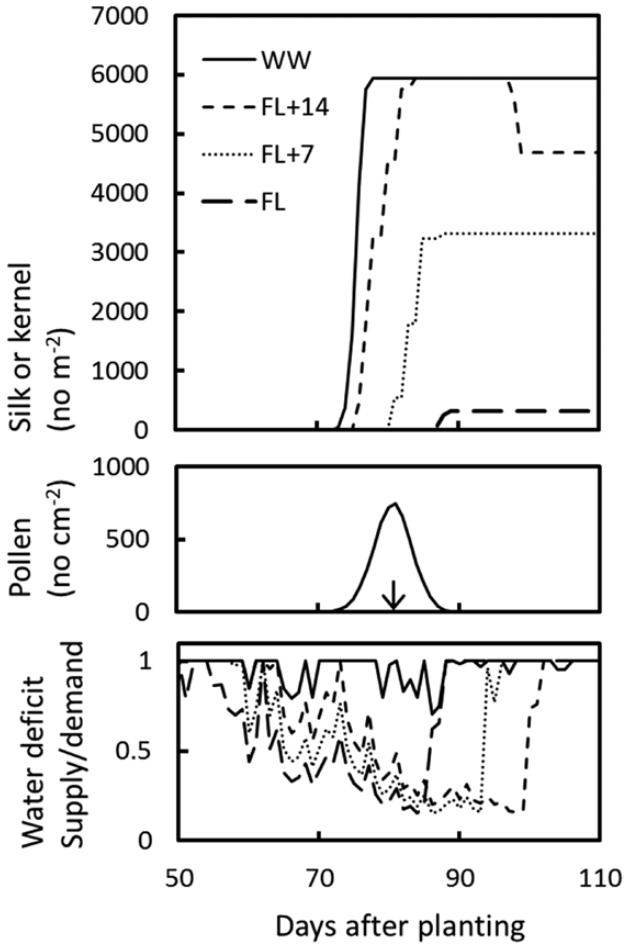

Figure 3. Simulated silk and kernel number, pollen counts and water deficit as characterized by the ratio between water supply and demand for treatments that were either well-watered (WW), or had maximum water deficit at 2 weeks after flowering (fl+14), 1 week after flowering (fl+7) or at flowering (fl). The arrow indicates the predicted timing of 50 % anthesis/pollen shedding.

flowering, or 1 or 2 weeks after flowering, immediately prior to the release of the water deficit by irrigation in those scenarios. Because time from planting to anthesis and pollen shedding did not differ among simulations, as it is little affected by water deficit, the temporal distribution of pollen supply was the same for all scenarios. However, the timing of silk emergence and increase in number, which occurred before 50 % flowering in the well-watered treatment, was delayed with increasing water deficit. This delay in silk appearance resulted in an increase in calculated ASI with increasing water deficit, as has been frequently observed (Bolaños and Edmeades 1996; Campos *et al.* 2006; Cooper *et al.* 2014). There was also a reduced rate of increase in silk number with increasing water deficit, which was associated with effects on silk elongation rate. Final silk, and hence kernel, number was most limited with severe water deficit at flowering time. In this condition, kernel set was affected by reduced silk numbers, silk elongation rate and limited pollen availability at the delayed time of silk emergence. Kernel abortion was only simulated when the maximum water deficit occurred 2 weeks after flowering and was a consequence of the combination of restricted assimilate availability and competition among developing kernels. These model behaviours are qualitatively consistent with those observed in practice under field conditions and controlled experiments (Claassen and Shaw 1970; Westgate and Boyer 1985b; Campos *et al.* 2006).

Simulated ASI correlated well with grain yield

The negative correlation between ASI and yield under stress conditions is well documented and the use of ASI as a selection criterion to improve drought tolerance in maize has been advocated in several reports (Bolaños and Edmeades 1996; Campos *et al.* 2006; Cooper *et al.* 2014). Causal relationships have been proposed to explain this association. A decrease in protandry improves the synchrony between silk emergence and exposure to fertile pollen (Hall *et al.* 1982). Alternative interpretations suggest that ASI is linked to ear growth (Edmeades *et al.* 1993), or that ASI is an indicator of plant health and nutritional and water status of silks, ovules and kernels (Hammer *et al.* 2009). The theoretical framework proposed here incorporates multiple causes that could lead to variations in silk emergence and ASI, including protandry and carbohydrate availability as well as the dynamics of the appearance of silks. Using the data generated in the structured simulation (Fig. 3), a clear relationship between ASI and yield emerges in a manner that conforms well to field-observed results (Fig. 4) (Bolaños and Edmeades 1996; Campos *et al.* 2006; Cooper *et al.* 2014). In this simulation experiment, the theoretical model generated this emergent relationship through failure in silk emergence, unsynchronized pollination and kernel abortion. A change in the silk elongation rate relative to the reference value was introduced to illustrate that results were not dependent on this specific simulation experiment.

The emergent relationship between simulated silk number and ear mass at silking reflected observed patterns

The dynamics of the maize pistillate flower have been related to plant growth (Borrás *et al.* 2007, 2009). Silk number increased with increasing plant growth rate (Borrás *et al.* 2007) or a form of its integral represented by the ear mass at silking (Cooper *et al.* 2014) (Fig. 5). Genotypic variation for a greater threshold ear mass at silking for silk emergence was shown to be associated

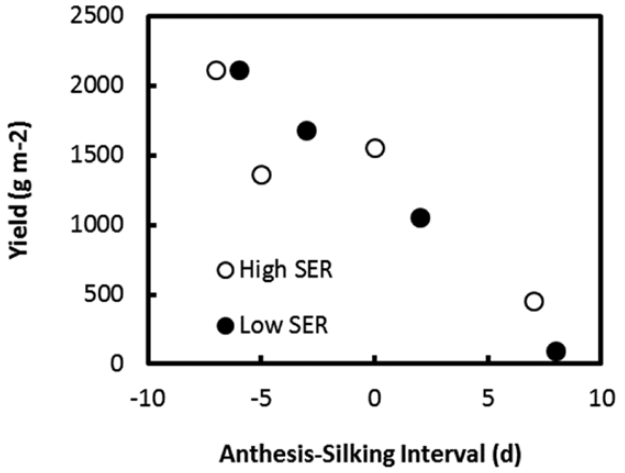

Figure 4. Simulated relationship between yield and ASI for two levels of silk elongation rate (SER).

with drought susceptibility in maize (Cooper *et al.* 2014). Under stress conditions and limited growth, low ear mass thresholds are associated with high elongation rate and synchronous silk appearance. Both synchronous floret growth and development, and pollination have been associated with reduced ovule and kernel abortion (Hall *et al.* 1982; Cárcova and Otegui 2001, 2007). Using the output data generated in the structured simulation (Fig. 3), the association between silk number and ear size at silking emerges (Fig. 5) and closely reflects the observed relationship. A simple model of the form $y = y_m \times (1 - e^{k \times (x - x_0)})$ can describe this association (Cooper *et al.* 2014). Parameter values estimated for both observed and simulated data (Fig. 5) suggest the model closely resembles the empirical association despite small but significant differences (y_m = 933 ± 42, k = 1.17 ± 0.1, x_0 = 1.2 ± 0.03, df = 68 vs. y_m = 906 ± 37, k = 1.48 ± 0.04, x_0 = 0.97 ± 0.02, df = 6). In this simulation experiment, the theoretical model generated this emergent relationship through the association between the effects of the extent of water deficit on both reduced growth and silk elongation and emergence.

The emergent relationship between simulated kernel number and plant growth rate around anthesis reflected observed patterns

The current paradigm to predict kernel set and yield in maize uses the association of kernel number with crop, plant or ear growth rate as an integrator of the health status of the plant (Andrade *et al.* 1999; Vega *et al.* 2001; Echarte *et al.* 2004). Andrade *et al.* (1999) showed that the relationship between kernel number per plant and plant growth rate around anthesis was robust across various factors limiting plant growth, such as levels of water, nitrogen and density stress. This relationship currently underpins prediction of

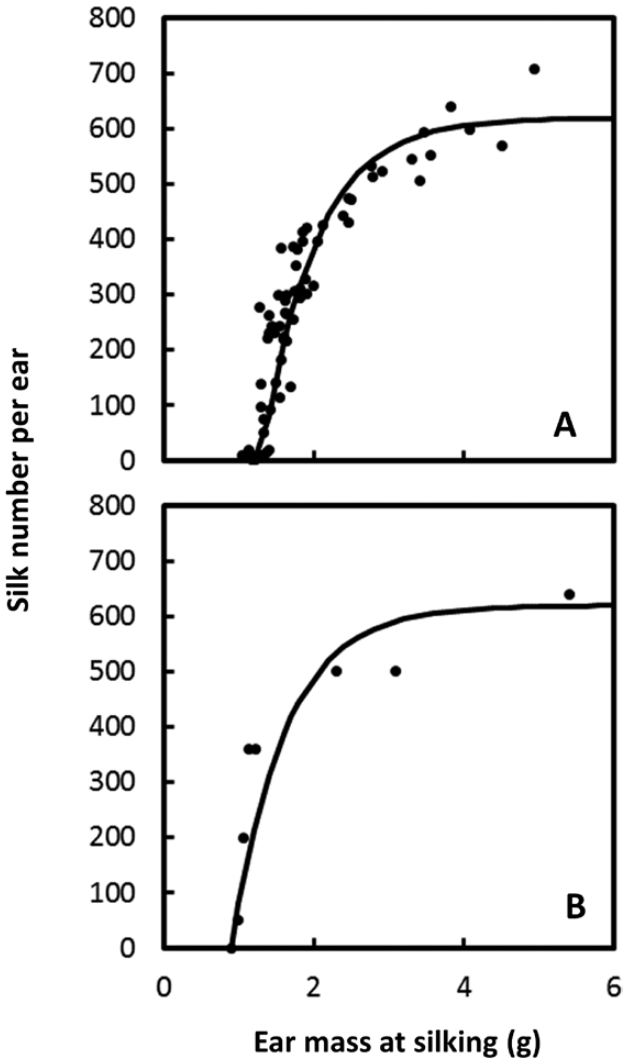

Figure 5. Observed (A) and simulated (B) association of silk number with ear mass at silking. Observed data are from Cooper *et al.* (2014). Parameters for the model $y = y_m \times (1 - e^{k \times (x - x_0)})$ are y_m = 933 ± 42, k = 1.17 ± 0.1, x_0 = 1.2 ± 0.03, df = 68 for the observed data (A), and y_m = 906 ± 37, k = 1.48 ± 0.04, x_0 = 0.97 ± 0.02, df = 6 for the simulated data (B).

maize yield in widely used crop growth models (CGMs) (Soufizadeh *et al.* 2018). From the structured simulation (Fig. 3), the association between kernel number and plant growth rate around anthesis is replicated (Fig. 6) as shown in a number of experimental studies. While the model was not parameterized to simulate the data shown in Fig. 6, it is possible to compute the distance between the simulated and the mean of observed values. The model predicts well the pattern of response (r = 0.88; n = 4) but with bias due to the overestimation of the plant growth rate at which kernel number equals 0 (1.44 vs. 0.74 ± 0.22 g per plant). In this simulation experiment, the emergent relationship from the theoretical model resulted from the

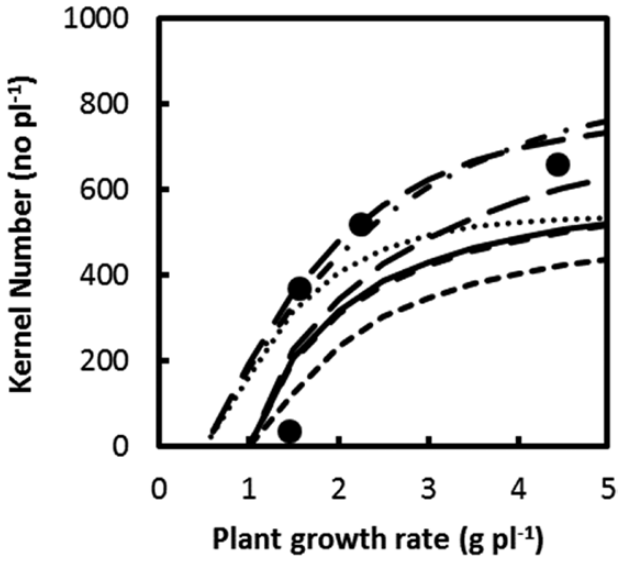

Figure 6. Simulated association between kernels per plant and average plant growth rate over a 20-day period bracketing anthesis (filled circles). Lines correspond to statistical models fitted to experimental data for different hybrids and years (Andrade *et al.* 1999; Vega *et al.* 2001; Echarte *et al.* 2004). Correlation calculated between simulated and mean observed kernel number (r = 0.88; n = 4). Observed plant growth rate at which kernel number equals 0 is 0.74 ± 0.22 g per plant.

association between the effects of the extent of water deficit on reduced plant growth in concert with effects on silk dynamics and kernel abortion.

Predictions of yield and yield components corresponded well with observations from specific field experiments with controlled patterns of water deficit

Impact of water deficit on maize yield depends on the synchrony between the stress and the development stage (Campos *et al.* 2006; Fig. 7). The detailed experiment of Campos *et al.* (2006) was utilized to evaluate the sensitivity of the model to timing of water deficit by examining the coherence of the simulation results with observations for the sample of historical hybrids used in the experiment. This sample of hybrids, spanning 47 years of commercial breeding, provides a range of attributes within which we should expect the integrated model to produce a simulation consistent with the observations as water deficit changed from well watered throughout the crop cycle to five treatments with overlapping water deficit windows imposed starting at flowering time (Campos *et al.* 2006). Details of the simulation set-up and results for each treatment are included in the **Supporting Information**. With a model parameterization based on the elite commercial drought-tolerant hybrid detailed in Hammer *et al.* (2009), the simulated results tracked well the observed response of yield and

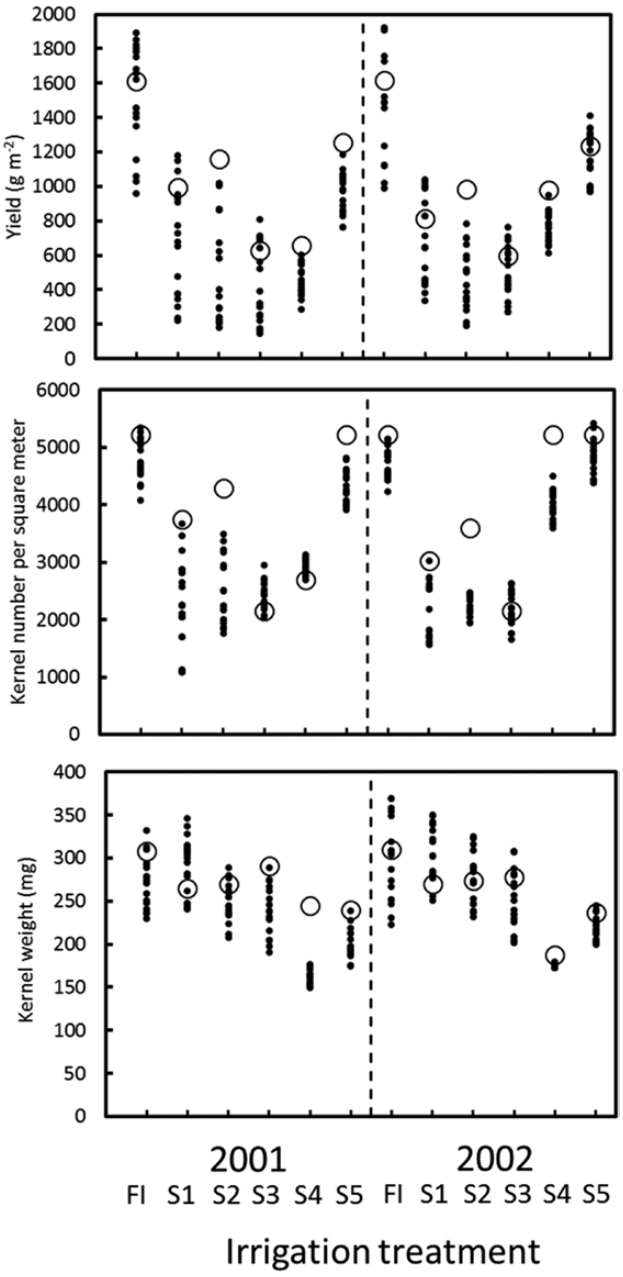

Figure 7. Impact of water deficit on maize yield and yield components when the stress was imposed at different stages of reproductive development (Campos *et al.* 2006). S1 and S2 indicate treatments with early and late flowering stress, and S3, S4 and S5 indicate treatments with early-mid, mid-late and late grain fill stress. FI is full irrigated. Closed symbols denote observations for all hybrids included in Campos *et al.* (2006). Open symbols denote values simulated with the integrated model. Correlation between the simulated and environment mean was 0.84 for kernel number, 0.74 for kernel weight and 0.89 for yield. Corresponding root mean square errors were 958 kernels per m^2, 36 mg and 293 g m^{-2}.

yield components to timing of water deficit. The correlation between the simulated trait and the mean across hybrids observed in a given environment (Fig. 7) was

0.84 for kernel number, 0.74 for kernel weight and 0.89 for yield. Corresponding root mean square errors were 958 kernels per m^2, 36 mg and 293 g m^{-2}. Due to genetic improvement across the hybrids studied, the observed range in yield and yield components for a given water treatment was large. The integrated model tended to simulate yield and yield components towards the high end of the distributions, which was consistent with expectations for the hybrid parameterized by Hammer *et al.* (2009).

In the simulation of this experiment, the reduced kernel number and yield associated with the S1 and S2 treatments (stress during early and late flowering) was generated by effects on silk extension and emergence **[see Supporting Information]**, whereas for the S3 treatment (stress during early-mid grain filling) it was generated by kernel abortion. For the S4 and S5 treatments (stress during mid-late and late grain filling) simulated yield reduction was associated with reduced kernel size. The simulated differential susceptibility to water deficit during grain filling was also consistent with other experimental data (Claassen and Shaw 1970; Westgate and Boyer 1985b; Westgate and Thompson Grant 1989).

Discussion

Reproductive failure in maize has long been studied in plant science. Seminal exploratory work by Claassen and Shaw (1970) suggested that the critical period for yield determination was around the emergence of the pistillate flowers. Since then, our understanding of the physiological and biochemical determinants of kernel set in maize under water limitation has been significantly advanced (Boyer 1996; Saini and Westgate 2000). More recent research suggests that developmental and growth synchrony is crucial to preventing kernel abortion (Cárcova and Otegui 2007; Oury *et al.* 2016). Both carbohydrate starvation, as believed for decades, and the direct effects of water limitation on the pattern of silk emergence, as discovered more recently, underpin kernel abortion in maize (Zinselmeier *et al.* 1995, 1999; Borrás *et al.* 2009; Oury *et al.* 2016).

Despite more than half a century of outstanding research on reproductive failure in maize, it has not been integrated into a quantitative dynamic framework that could enable prediction of emergent properties based on the current understanding of the driving component biological processes. The quantitative synthesis presented here demonstrates a capacity to capture emergent behaviour typical of complex systems (Hammer *et al.* 2006) in a manner that corresponds well with empirical observations. While further empirical evaluation is needed to estimate metrics to quantify predictability of states such as yield (Wallach *et al.* 2018), the results demonstrate that it is possible to predict functional relations and phenotypic responses as emergent properties of the plant system based on the interplay of the physiological processes formalized in the underpinning set of equations and integrated in CGMs (Hammer *et al.* 2006; Messina *et al.* 2009). Future experimentation should produce adequate and independent data sets to test predictions of emergent phenotypes from ovule to yield under contrasting environments.

This quantitative dynamic framework is a significant advance from previous descriptive methods developed to predict kernel set and reproductive failure in maize (Andrade *et al.* 1999; Vega *et al.* 2001; Echarte *et al.* 2004; Lizaso *et al.* 2007; Soufizadeh *et al.* 2018). Research on reproductive failure has largely ignored system dynamics other than for the synchronization of reproductive processes such as pistillate flower development and pollination (Cárcova and Otegui 2001, 2007; Oury *et al.* 2016). Understanding the role of system dynamics in determining emergent phenotypes in whole plant biology and crop science is still in its infancy (Hammer *et al.* 2006). This synthesis can motivate further research that could be integrated with the current work to advance our collective effort on the fundamental concepts in biology that underpin the expression of phenotypes, phenotypic plasticity and phenotypic variation.

Linking genotypes to phenotypes, and to fitness and adaptation landscapes, can be traced to the early work by Fisher and Wright (Orr 2005). The current synthesis provides a framework to study the genetic architecture of reproductive failure in maize. Genotypes can generate smooth or rugged adaptation landscapes (Messina *et al.* 2011) depending on the connectivity and structure of the system of equations that govern the expression of the trait and its response to environmental variation. Here we have shown an example of the smooth correlation generated between ASI and yield, which is very well documented. However, the association emerges from the expression of failure in silking and/or abortion, depending on the timing of the environmental perturbation, the biological processes taking place at the time of the perturbation and the competition among reproductive sinks. The search for and use of a single signal and determinant of reproductive failure is likely to lead to low predictability of maize performance under stress. Prediction frameworks such as presented in this research, that incorporate determinants and processes generating system dynamics, are likely to direct to a more productive path to enhanced genetic prediction that drives genetic gain (Messina *et al.* 2018). Worthwhile future

studies will seek to quantify the sensitivity of emergent phenotypes (e.g. ASI, yield) generated by the model within well-defined environment-by-management systems by means of breeding simulation (Hammer *et al.* 2006; Messina *et al.* 2009), yield-trait performance landscapes (Messina *et al.* 2011) or sensitivity analyses (Hammer *et al.* 2009; Wallach *et al.* 2018).

Technology revolutions in genomics and phenomics are enabling the exploration of genomes and phenomes in unprecedented ways (Houle *et al.* 2010; Fahlgren *et al.* 2015). However, analytical methodologies grounded on causal biological relations to enable linking such vast data sets for predictive purposes are lacking. The quantitative synthesis presented here is an example of a hierarchical model that bridges high-level phenotypes, such as yield, with process-level phenotypes, such as silk elongation response to water deficit. By doing so it reduces the phenotypic distance between causal and emergent phenotypes and facilitates the connection between genomics and phenomics (Hammer *et al.* 2016), increases the predictability of plant systems (Messina *et al.* 2018) and enables prediction in agriculture. Predictive agriculture is in the end the discipline that will support translating plant biology understanding, measurement systems and mathematical modelling into decisions that will improve human well-being. Predictive agriculture can also help generate testable hypotheses to advance plant science. Here, we have presented a synthesis of reproductive failure in maize, which shows how we can progress dynamic modelling to translate biology into decision-making by leveraging fundamental biological knowledge. It provides pathways to improve crops through molecular breeding (Cooper *et al.* 2014) and genome-editing technologies (Svitashev *et al.* 2016) that have potential to help ameliorate the vast societal consequences of reproductive failure in maize.

Sources of Funding

EU-DROPS Consortium and Australian Research Council Linkage Project 100100495.

Conflict of Interest

C.D.M. and C.G. are employed by Corteva Agriscience, Agricultural Division of DowDuPont.

Acknowledgements

The authors acknowledge EU-DROPS Consortium and Australian Research Council Linkage Project 100100495 for supporting F.T., G.L.H., G.M., E.J.v.O., S.C.C. and A.D. and facilitating collaboration among groups thorough modelling workshops.

Supporting Information

The following additional information is available in the online version of this article—

Table S1. Definition of equation components (Parameter/Variable), units and representative values for the hybrid as used for the simulation of the field experiment.

Figure S1. Daily weather (minimum and maximum temperature, rainfall, solar radiation) for the field experiments at Viluco in 2001 and 2002.

Literature Cited

Anderson SR, Lauer MJ, Schoper JB, Shibles RM. 2004. Pollination timing effects on kernel set and silk receptivity in four maize hybrids. *Crop Science* **44**:464–473.

Andrade FH, Vega C, Uhart S, Cirilo A, Cantarero M, Valentinuz O. 1999. Kernel number determination in maize. *Crop Science* **39**:453–459.

Bassetti P, Westgate ME. 1993. Emergence, elongation, and senescence of maize silks. *Crop Science* **33**:271–275.

Bassetti P, Westgate ME. 1994. Floral asynchrony and kernel set in maize quantified by image analysis. *Agronomy Journal* **86**:699–703.

Birch CJ, Hammer GL, Rickert KG. 1998a. Temperature and photoperiod sensitivity of development in five cultivars of maize (*Zea mays* L.) from emergence to tassel initiation. *Field Crops Research* **55**:93–107.

Birch CJ, Hammer GL, Rickert KG. 1998b. Modelling leaf production and crop development in maize (*Zea mays* L.) after tassel initiation under diverse conditions of temperature and photoperiod. *Field Crops Research* **58**:81–95.

Bolaños J, Edmeades GO. 1996. The importance of the anthesis-silking interval in breeding for drought tolerance in tropical maize. *Field Crops Research* **48**:65–80.

Borrás L, Astini JP, Westgate ME, Severini A. 2009. Modeling anthesis to silking in maize using a plant biomass framework. *Crop Science* **49**:937–948.

Borrás L, Westgate ME, Astini JP, Echarte L. 2007. Coupling time to silking with plant growth rate in maize. *Field Crops Research* **102**:73–85.

Boyer JS. 1996. Advances in drought tolerance in plants. *Advances in Agronomy* **56**:187–217.

Boyer JS, Byrne P, Cassman KG, Cooper M, Delmer D, Greene T, Gruis F, Habben J, Hausmann N, Kenny N, Lafitte R, Paszkiewicz S, Porter D, Schlegel A, Schussler J, Setter T, Shanahan J, Shar RE, Vyn TJ, Warner D, Gaffney J. 2013. The U.S. drought of 2012 in perspective: a call to action. *Global Food Security* **2**:139–143.

Campos H, Cooper M, Edmeades GO, Löffler C, Schussler JR, Ibañez M. 2006. Changes in drought tolerance in maize associated with fifty years of breeding for yield in the U.S. Corn Belt. *Maydica* **51**:369–381.

Cane MA, Eshel G, Buckland RW. 1994. Forecasting Zimbabwean maize yield using eastern equatorial Pacific sea surface temperature. *Nature* **370**:204–205.

Cárcova J, Andrieu B, Otegui ME. 2003. Silk elongation in maize: relationship with flower development and pollination. *Crop Science* **43**:914–920.

Cárcova J, Otegui ME. 2001. Ear temperature and pollination timing effects on maize kernel set. *Crop Science* **41**:1809–1815.

Cárcova J, Otegui ME. 2007. Ovary growth and maize kernel set. *Crop Science* **47**:1104–1110.

Cárcova J, Uribelarrea M, Borrás L, Otegui ME, Westgate ME. 2000. Synchronous pollination within and between ears improves kernel set in maize. *Crop Science* **40**:1056–1061.

Claassen MM, Shaw RH. 1970. Water deficit in corn. II. Grain components. *Agronomy Journal* **62**: 652–655.

Cooper M, Messina CD, Podlich D, Radu Totir L, Baumgarten A, Hausmann NJ, Wright D, Graham G. 2014. Predicting the future of plant breeding: complementing empirical evaluation with genetic prediction. *Crop & Pasture Science* **65**:311–336.

Echarte L, Andrade FH, Vega CRC, Tollenaar M. 2004. Kernel number determination in Argentinean maize hybrids released between 1965 and 1993. *Crop Science* **44**:1654–1661.

Edmeades GO, Hernandez JBM, Bello S. 1993. Causes for silk delay in a lowland tropical maize population. *Crop Science* **33**:1029–1035.

Fahlgren N, Gehan MA, Baxter I. 2015. Lights, camera, action: high-throughput plant phenotyping is ready for a close-up. *Current Opinion in Plant Biology* **24**:93–99.

Fuad-Hassan A, Tardieu F, Turc O. 2008. Drought-induced changes in anthesis-silking interval are related to silk expansion: a spatio-temporal growth analysis in maize plants subjected to soil water deficit. *Plant, Cell & Environment* **31**:1349–1360.

Gambín BL, Borrás L, Otegui ME. 2008. Kernel weight dependence upon plant growth at different grain-filling stages in maize and sorghum. *Australian Journal of Agricultural Research* **59**:280–290.

Hall AJ, Vilella F, Trapani N, Chimenti C. 1982. The effects of water stress and genotype on the dynamics of pollen-shedding and silking in maize. *Field Crops Research* **5**:349–363.

Hammer G, Cooper M, Tardieu F, Welch S, Walsh B, van Eeuwijk F, Chapman S, Podlich D. 2006. Models for navigating biological complexity in breeding improved crop plants. *Trends in Plant Science* **11**:587–593.

Hammer GL, Dong Z, McLean G, Doherty A, Messina C, Schussler J, Zinselmeier C, Paszkiewicz S, Cooper M. 2009. Can changes in canopy and/or root system architecture explain historical maize yield trends in the U.S. Corn Belt? *Crop Science* **49**:299–312.

Hammer GL, McLean G, Chapman S, Zheng B, Doherty A, Harrison MT, van Oosterom E, Jordan D. 2014. Crop design for specific adaptation in variable dryland production environments. *Crop & Pasture Science* **65**:614–626.

Hammer G, Messina C, van Oosterom E, Chapman S, Singh V, Borrell A, Jordan D, Cooper M. 2016. Molecular breeding for complex adaptive traits – how integrating crop ecophysiology and modelling can enhance efficiency. In: Yin X, Struik P, eds. *Crop systems biology: narrowing the gap between genotype and phenotype*. Cham, Switzerland: Springer International Publishing, 147–162.

Hammer GL, van Oosterom E, McLean G, Chapman SC, Broad I, Harland P, Muchow RC. 2010. Adapting APSIM to model the physiology and genetics of complex adaptive traits in field crops. *Journal of Experimental Botany* **61**:2185–2202.

Herrero MP, Johnson RR. 1980. High temperature stress and pollen viability of maize. *Crop Science* **20**:796–800.

Herrero MP, Johnson RR. 1981. Drought stress and its effects on maize reproductive systems. *Crop Science* **21**:105–110.

Holzworth DP, Huth NI, deVoil PG, Zurcher EJ, Herrmann NI, McLean G, Chenu K, van Oosterom E, Snow V, Murphy C, Moore AD, Brown H, Whish JPM, Verrall S, Fainges J, Bell LW, Peake AS, Poulton PL, Hochman Z, Thorburn P, Gaydon DS, Dalgliesh NP, Rodriguez D, Cox H, Chapman S, Doherty A, Teixeira E, Sharp J, Cichota R, Vogeler I, Li FY, Wang E, Hammer GL, Robertson MJ, Dimes JP, Whitbread AM, Hunt J, van Rees H, McClelland T, Carberry PS, Hargreaves JNG, MacLeod N, McDonald C, Harsdorf J, Wedgwood S, Keating BA. 2014. APSIM-evolution towards a new generation of agricultural systems simulation. *Environmental Modelling and Software* **62**:327–350.

Houle D, Govindaraju DR, Omholt S. 2010. Phenomics: the next challenge. *Nature Reviews Genetics* **11**:855–866.

Kiniry JR, Bonhomme R. 1991. Predicting maize phenology. In: Hodges T, ed. *Predicting crop phenology*. Boca Raton, FL: CRC Press, 115–132.

Lizaso JI, Fonseca AE, Westgate ME. 2007. Simulating source-limited and sink-limited kernel set with CERES-maize. *Crop Science* **47**:2078–2088.

Messina C, Hammer G, Dong Z, Podlich D, Cooper M. 2009. Modelling crop improvement in a G*E*M framework via gene-trait-phenotype relationships. In: Sadras VO, Calderini DF, eds. *Crop physiology: applications for genetic improvement and agronomy*. London, UK: Academic Press, 235–266.

Messina CD, Podlich D, Dong Z, Samples M, Cooper M. 2011. Yield-trait performance landscapes: from theory to application in breeding maize for drought tolerance. *Journal of Experimental Botany* **62**:855–868.

Messina CD, Technow F, Tang T, Totir R, Gho C, Cooper M. 2018. Leveraging biological insight and environmental variation to improve phenotypic prediction: integrating crop growth models (CGM) with whole genome prediction (WGP). *European Journal of Agronomy* **100**:151–162.

Moss GI, Downey LA. 1971. Influence of drought stress on female gametophyte development in corn. *Crop Science* **11**:368–372.

Muchow RC. 1990. Effect of high temperature on grain-growth in field-grown maize. *Field Crops Research* **23**:145–158.

Orr HA. 2005. The genetic theory of adaptation: a brief history. *Nature Reviews Genetics* **6**:119–127.

Otegui ME, Melon S. 1997. Kernel set and flower synchrony within the ear of maize: I. sowing date effects. *Crop Science* **37**:441–447.

Oury V, Tardieu F, Turc O. 2016. Ovary apical abortion under water deficit is caused by changes in sequential development of ovaries and in silk growth rate in maize. *Plant Physiology* **171**:986–996.

Ray DK, Gerber JS, MacDonald GK, West PC. 2015. Climate variation explains a third of global crop yield variability. *Nature Communications* **6**:5989.

Ray DK, Mueller ND, West PC, Foley JA. 2013. Crop Yield trends are insufficient to double global food production by 2050. *PLoS One* **8**:e66428.

Saini HS, Westgate ME. 2000. Reproductive development in grain crops during drought. *Advances in Agronomy* **68**:59–95.

Schoper JB, Lambert RJ, Vasilas BL, Westgate ME. 1987. Plant factors controlling seed set in maize: the influence of silk, pollen, and ear-leaf water status and tassel heat treatment at pollination. *Plant Physiology* **83**:121–125.

Singh V, Nguyen CT, McLean G, Chapman SC, Zheng B, van Oosterom EJ, Hammer GL. 2017. Quantifying high temperature risks and their potential effects on sorghum production in Australia. *Field Crops Research* **211**:77–88.

Soufizadeh S, Munaro E, McLean G, Massignam, A, van Oosterom EJ, Chapman SC, Messina C, Cooper M, Hammer GL. 2018. Modelling the nitrogen dynamics of maize crops – enhancing the APSIM maize model. *European Journal of Agronomy* **100**:118–131.

Svitashev S, Schwartz C, Lenderts B, Young JK, Mark Cigan A. 2016. Genome editing in maize directed by CRISPR-Cas9 ribonucleoprotein complexes. *Nature Communications* **7**:13274.

Turc O, Bouteillé M, Fuad-Hassan A, Welcker C, Tardieu F. 2016. The growth of vegetative and reproductive structures (leaves and silks) respond similarly to hydraulic cues in maize. *The New Phytologist* **212**:377–388.

Uribelarrea M, Cárcova J, Otegui ME, Westgate ME. 2002. Pollen production, pollination dynamics, and kernel set in maize. *Crop Science* **42**:1910–1918.

Vega CRC, Andrade FH, Sadras VO, Uhart SA, Valentinuz OR. 2001. Seed number as a function of growth. A comparative study in soybean, sunflower and maize. *Crop Science* **41**:748–754.

Wallach D, Makowski D, Brun F, Jones JW. 2018. *Working with dynamic crop models: methods, tools and examples for agriculture and environment*, 3rd edn. London, UK: Academic Press.

Westgate ME, Boyer JS. 1985a. Osmotic adjustment and the inhibition of leaf, root, stem and silk growth at low water potentials in maize. *Planta* **164**:540–549.

Westgate ME, Boyer JS. 1985b. Carbohydrate reserves and reproductive development at low leaf water potentials in maize. *Crop Science* **25**:762–769.

Westgate ME, Boyer JS. 1986. Reproduction at low silk and pollen water potentials in maize. *Crop Science* **26**:952–956.

Westgate ME, Grant DL. 1989. Water deficits and reproduction in maize: response of the reproductive tissue to water deficits at anthesis and mid-grain fill. *Plant Physiology* **91**:862–867.

Wilson DR, Muchow RC, Murgatroyd CJ. 1995. Model analysis of temperature and solar radiation limitations to maize potential productivity in a cool climate. *Field Crops Research* **43**:1–18.

Zinselmeier C, Jeong BR, Boyer JS. 1999. Starch and the control of kernel number in maize at low water potentials. *Plant Physiology* **121**:25–36.

Zinselmeier C, Westgate ME, Schussler JR, Jones RJ. 1995. Low water potential disrupts carbohydrate metabolism in maize (*Zea mays* L.) ovaries. *Plant Physiology* **107**:385–391.

